

Thermal History of Solid ^4He Under Oscillation

A. C. Clark,* J. D. Maynard, and M. H. W. Chan

Department of Physics, The Pennsylvania State University, University Park, Pennsylvania 16802

(Dated: February 9, 2022)

We have studied the thermal history of the resonant frequency of a torsional oscillator containing solid ^4He . We find that the magnitude of the frequency shift that occurs below ~ 100 mK is multi-valued in the low temperature limit, with the exact value depending on how the state is prepared. This result can be qualitatively explained in terms of the motion and pinning of quantized vortices within the sample. Several aspects of the data are also consistent with the response of dislocation lines to oscillating stress fields imposed on the solid.

PACS numbers: 67.80.-s, 61.72.Lk, 74.25.Qt

I. INTRODUCTION

Over the last several years the torsional oscillator (TO) technique has become a popular method^{1,2,3,4,5,6,7,8,9,10,11,12} to study solid ^4He . The measurements, which involve monitoring the resonant frequency f of a high quality factor torsion pendulum filled with ^4He , have revealed a “transition” below an onset temperature T_O of ~ 200 mK. The results of several control experiments² indicate that the sudden increase in the frequency is due to a superfluid-like decoupling of a fraction of the ^4He mass. The apparent nonclassical rotational inertia fraction (NCRIF), proportional to the frequency shift δf , is independent² of the maximum oscillation speed v_0 of the TO provided that it is smaller than a critical value. Above this critical velocity v_C the magnitude of NCRIF is attenuated. The value of v_C corresponds to several quanta of circulation κ , suggesting that the important excitations in the system are vortices. Anderson has proposed¹³ a vortex liquid model that qualitatively captures a number of experimental results.

In multiple solid ^4He samples slowly grown within an annulus of radius, $r = 5$ mm, and width¹⁴, $t = 0.95$ mm, a value of $v_C = 10 \mu\text{m s}^{-1}$ was found⁴ (corresponding to $\kappa = 2\pi r v_0 \approx 3h/m$, where h is Planck’s constant and m is the bare ^4He mass). NCRIF decreased almost linearly with $\ln[v_0]$ as the speed was increased further. This attenuation, according to Ref. 13, is attributable to the nonlinear susceptibility of a vortex liquid phase, which consists of an entanglement of many thermally activated vortices¹³. The ability of the vortices to move counter to the time-dependent superflow (relative to the cell’s oscillation) results in the screening of supercurrents. As the temperature is lowered the motion and number of vortices is reduced so that NCRIF becomes finite. The accompanying dissipation² that peaks in the middle of the transition is due to a matching of f and the optimal rate at which vortices respond to changes in the velocity field. Residual ^3He atoms may¹⁵ cling to vortices, thereby slowing vortex motion and ultimately enhancing the onset temperature^{1,10,11}.

One prediction of Anderson’s model¹³ is that T_O , and perhaps NCRIF, for a particular sample will decrease

as the measurement frequency is lowered. Aoki *et al.* performed⁷ measurements in a double oscillator that operated in either an antisymmetric (high f) or a symmetric (low f) mode and found that for the same ^4He sample, $T_O \approx 240$ mK at 1173 Hz and $T_O \approx 160$ mK at 496 Hz. However, NCRIF became independent of frequency below ~ 35 mK. In addition, irreversible changes in NCRIF below ~ 45 mK occurred upon variation of the oscillation speed between $10 \mu\text{m s}^{-1}$ and $800 \mu\text{m s}^{-1}$.

Nonsuperfluid explanations of the TO experiments have also been proposed, in which some sort of freezing process¹⁶ or glass transition¹⁷ takes place. Although the former was only discussed qualitatively, the pinning of dislocation lines within solid ^4He is one possible realization of such a “freezing” transition. The mechanism for dislocation pinning is likely related to interactions with isotopic impurities. It is known that dislocations¹⁸ and ^3He atoms^{19,20} are mobile in solid ^4He below ~ 1 K, but the strong coupling between them in the low temperature limit can immobilize them both^{21,22}. In a TO study¹¹ of many solid ^4He samples we found that the dependence of T_O on the ^3He concentration x_3 is quantitatively consistent with this impurity-pinning model.

Recently Day and Beamish observed²³ a dramatic increase (between 5% and 20%) in the shear modulus c_{44} of solid ^4He ($x_3 \approx 0.3$ ppm) below ~ 250 mK, with the temperature dependence of c_{44} strongly resembling that of f in TO experiments. The authors also reported hysteresis in c_{44} upon adjusting the stress amplitude of the measurement at $T \approx 20$ mK, similar to what is seen in Ref. 7. The increase in the shear modulus is very likely due to the stiffening of the dislocation network via the immobilization of individual lines. It was suggested by the authors of Ref. 23 that an increase in c_{44} will result in a stronger coupling between the ^4He sample and its container and therefore mimic an enhanced mass loading of a TO, causing f to decrease. However, any enhancement to the overall rigidity of the system actually leads to a higher resonant frequency. We have carried out a finite element method (FEM) calculation²⁴ employing realistic parameters of the TO and solid helium in order to confirm this result. The positive correlation between c_{44} and f ; their resemblances in the temperature dependence, and the hysteresis common to both, all suggest that either the

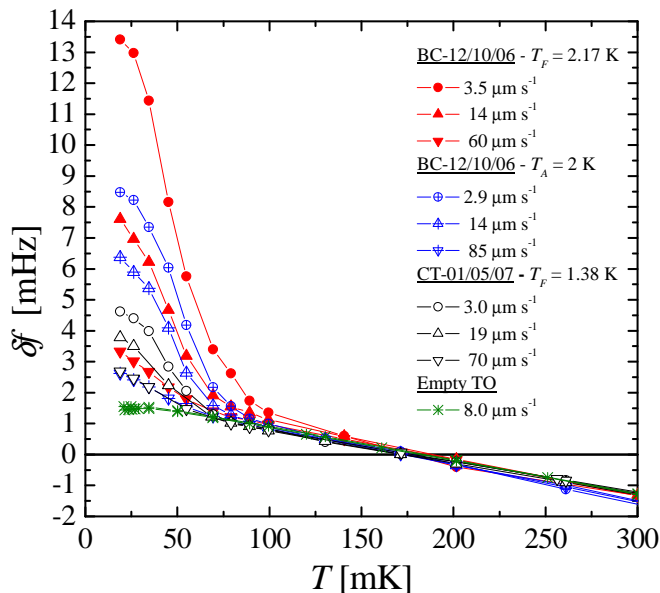


FIG. 1: Temperature dependence of δf for a BC sample before and after annealing, and one CT sample. For all samples $x_3 \approx 1$ ppb. Data was obtained with the beryllium-copper TO from Ref. 10. Freezing (T_F) and annealing (T_A) temperatures are given for each sample. All data was taken during cooling scans in which the temperature was successively lowered in controlled steps. For any one sample the measured frequency at $T > T_O$ is identical for all values of v_0 . For easy comparison we have set $\delta f = 0$ at $T = 175$ mK by subtracting 1071.007 Hz, 1071.011 Hz, 1071.035 Hz, and 1071.898 Hz from the data of BC-12/10/06, BC-12/10/06 post-annealing, CT-010507, and the empty TO. Thus, the effective mass loading for each of these samples is 891 mHz, 887 mHz, and 863 mHz.

frequency shift is a direct consequence of the enhanced modulus and can be explained without invoking supersolidity or that the microscopic mechanism responsible for NCRIF also affects the elastic properties of the solid (e.g., a recent suggestion is given in Ref. 25). The results presented below appear to favor the latter.

Sec. II we present our experimental observations in a general manner by simply describing the dependencies of the observed frequency shifts and dissipation signals on temperature (see Figs. 1 and 2), oscillation speed²⁶ (see Fig. 3), and growth method. Two different interpretations of the data are given in Secs. III and IV. In the former we attempt to describe the experiments in the context of a supersolid that is permeated by vortices. Since vortex lines interact with velocity fields one of the important parameters in this model is v_0 . In Sec. IV we discuss the consequences of attributing the entire frequency shift to an increase in the shear modulus of solid ^4He . It is assumed in this picture that the rigidity of the solid is strongly affected by the motion of dislocation lines under the applied stress σ . In anticipation of these two interpretations, we have simultaneously plotted the data in Fig. 3 as a function of v_0 and σ . In addition, in

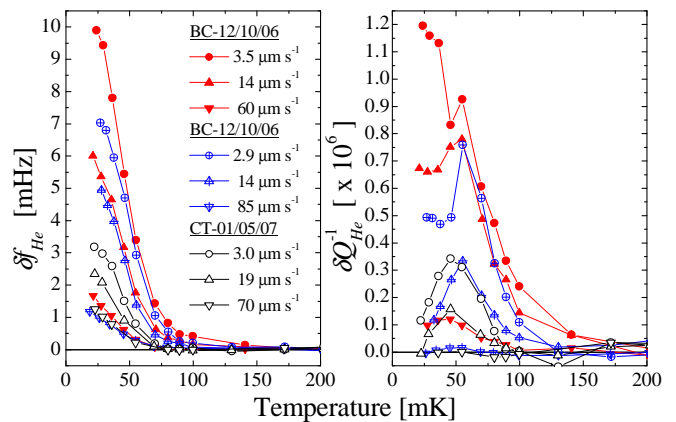


FIG. 2: Temperature dependence of δf_{He} and $\delta Q_{\text{He}}^{-1}$ for the same samples presented in Fig. 1, obtained by subtracting the temperature dependence of the empty cell. The symbols for BC-12/10/06, pre- and post-annealing, are identical to those in Fig. 1.

both Figs. 4 and 5 we have plotted the frequency shift in terms of NCRIF and $\delta c_{44}/c_{44}$.

II. EXPERIMENTAL RESULTS

A recent study¹⁰ of samples grown at constant temperature and pressure (CT/CP) at a single point on the solid-liquid coexistence curve found the onset of the frequency shift to be sharp and reproducible, which is consistent with the expected formation of single crystals. In contrast, wide variations in δf and T_O were observed when employing the blocked capillary (BC) method, which typically yields polycrystalline samples or highly strained crystals due to the pressure drop during freezing. In this paper we examine in detail the different thermal histories of δf in BC and CT/CP samples that follow from changes in oscillation speed above and below T_O . We have measured the temperature dependence of δf in 30 samples, with the bulk of our work being carried out on “isotopically pure” ($x_3 \approx 1$ ppb of ^3He) samples at $1 \mu\text{m s}^{-1} < v_0 < 100 \mu\text{m s}^{-1}$. To overlap with Ref. 7 we also studied commercially pure ($x_3 \approx 0.3$ ppm) samples up to speeds of $880 \mu\text{m s}^{-1}$.

Figure 1 shows the temperature dependence of δf for a BC sample before and after annealing, compared with that for a sample grown at CT. We find that the temperature dependence of δf for each sample is reproducible in warming and cooling scans at low oscillation speeds, i.e., on the order of one micron per second. Although the differences between BC and CT/CP samples are apparent at low speeds, the temperature dependence obtained at $v_0 > 50 \mu\text{m s}^{-1}$ is very similar in all samples studied (including 0.3 ppm samples).

After subtracting the temperature dependence of the empty cell we obtain the frequency shift and dissipation due to solid ^4He , which we respectively denote by δf_{He}

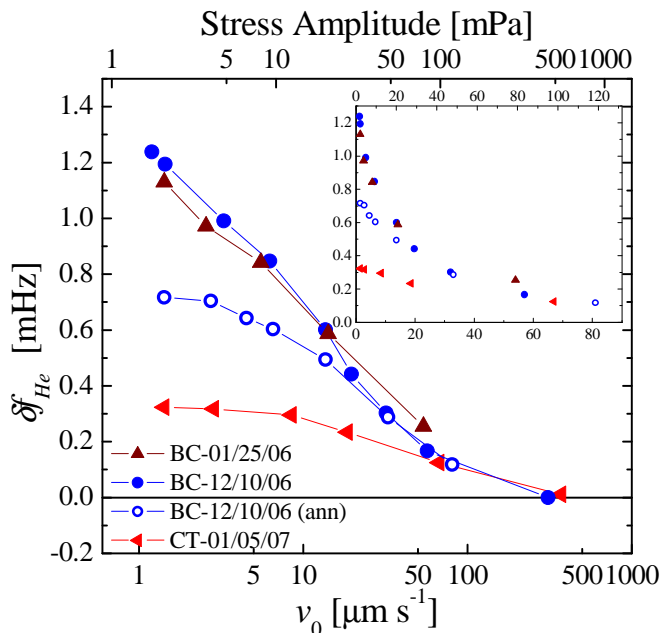


FIG. 3: Dependence of the low temperature value of δf_{He} on oscillation speed and applied stress. The inertial stress is approximated by $\sigma \approx \pi \rho f v_0 / 2$, for a given helium density ρ . Values of f_{He} were extracted from cooling scans that began well above T_O . Samples are labeled according to growth method and date. The data are plotted versus a linear abscissa in the inset.

and δQ_{He}^{-1} . These results are plotted in Fig. 2. There is considerable dissipation in rapidly grown BC samples even at the lowest temperatures. After annealing sample BC-12/10/06 the high temperature tail of δf_{He} (and thus T_O), the low temperature limiting value of δf_{He} , and the magnitude of δQ_{He}^{-1} are all reduced. Thus it appears that annealing affects the temperature dependence of δf_{He} much in the same way as driving the TO at high speed (see Fig. 2). One difference, however, is that the results from annealing are permanent.

In Fig. 3 we have plotted the low temperature value of δf_{He} measured at different v_0 , which again demonstrates that the data converge at high speeds. One interesting difference from previous TO studies^{2,4,6,7,8} is the lack of saturation in δf_{He} even well below $10 \mu\text{m s}^{-1}$. This is most evident in two BC samples (01/25/07 and 12/10/06) grown from the normal fluid phase, where δf_{He} actually doubles when v_0 is decreased from $10 \mu\text{m s}^{-1}$ to $1 \mu\text{m s}^{-1}$. In samples assumed to be of higher quality, we find $v_C \approx 3 \mu\text{m s}^{-1}$ ($3.5 \mu\text{m s}^{-1}$ corresponds to $\kappa = h/m$).

The curves in Fig. 3 were compiled from cooling scans that began well above the onset temperature. Using this procedure we found that δf_{He} is diminished at higher v_0 for all $T < T_O$ in a completely reproducible manner, whereas measurements taken during warming are history-dependent when obtained at speeds greater than a few microns per second. As we will show below, varying

the oscillation speed below the onset temperature can result in irreversible changes in δf_{He} . Careful examination of how the oscillation speed affects δf_{He} reveals metastability at the lowest temperatures, as depicted in Figs. 4 and 5 (see Secs. III and IV).

Using the following protocol, the thermal history of δf_{He} was investigated in crystals grown under different conditions. First, the temperature dependence of δf_{He} was measured while cooling at low speed ($v_0 < 3 \mu\text{m s}^{-1}$). At $T \approx 20 \text{ mK}$ v_0 was slowly increased. Final velocities were usually $\sim 20 \mu\text{m s}^{-1}$, but in some cases much greater (e.g., several hundred microns per second). Multiple thermal cycles were then performed in succession, indicated by the arrows in Fig. 4. Complete equilibration was purposely avoided while cycling between 30 mK and 60 mK in order to observe multiple metastable states. The measurement culminated with a high velocity cooling trace that began well above T_O .

Figures 4 and 5 show that for one oscillation speed a number of different values of δf_{He} ($\propto \text{NCRIF}$ and $\delta c_{44}/c_{44}$) can be “frozen in” below a characteristic temperature, $T^* \approx 30 \text{ mK}$. This is true regardless of the sample growth procedure. However, there are significant differences in the time evolution (following temperature steps) and the velocity dependence of δf_{He} between samples formed by the BC method and crystals grown at CT/CP. Similar behavior is seen in 0.3 ppm samples, but with $T^* \approx 45 \text{ mK}$. For all samples, there is no observable decay from any of the metastable states of δf_{He} on a timescale of days as long as the temperature is maintained below T^* . Further discussion of the hysteresis is deferred to Secs. III and IV below.

III. THE VORTEX LIQUID MODEL

As stated in Sec. I, the TO experiments to date are qualitatively consistent with many features of Anderson’s vortex liquid model. The present work, however, demonstrates that below 60 mK the system does not act like a free vortex liquid as originally proposed. In fact, below 30 mK it exhibits severe pinning. With this picture in mind we can explain the temperature dependence of NCRIF ($\propto \delta f_{He}$) in Fig. 2, the velocity dependence in Fig. 3, and the history dependence in Figs. 4 and 5.

First we consider the temperature dependence. As the system is cooled through the transition some number of free vortices are produced, which is proportional to v_0 . When $T \ll T_O$ the mobility of the existing vortices diminishes and it is unfavorable to create additional vortex lines. The inability of vortices to screen supercurrents leads to a sizeable NCRIF in the low temperature limit. When the system is driven at high speeds, not only is NCRIF smaller but the high temperature tail of NCRIF is reduced. This suggests that vortex pinning is very weak at $T \geq 60 \text{ mK}$. It is also likely that vortices are more easily excited as T_O is approached.

The velocity dependence in Fig. 3 reflects the distri-

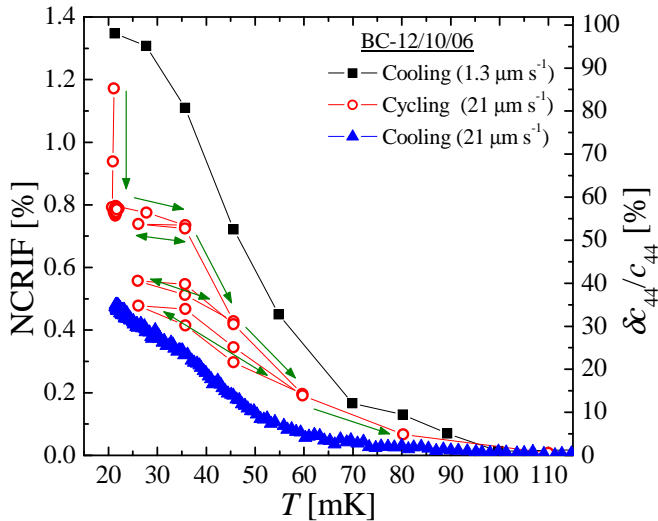


FIG. 4: Metastability of δf_{He} (plotted as NCRIF and $\delta c_{44}/c_{44}$) for a BC sample. The values of $\delta c_{44}/c_{44}$ were calculated based on the assumption that the solid sample was isotropic, i.e., highly polycrystalline²⁷ due to BC method that was employed. Even larger values would be obtained if the sample was assumed to be a single crystal. Decay of the signal occurs for $T > 30$ mK. Cycling above and below $T^* = 30$ mK results in successively smaller values until equilibrium (i.e., that obtained when cooling from above T_0) is reached. The speeds of $v_0 = 1.3 \mu\text{m s}^{-1}$ and $21 \mu\text{m s}^{-1}$ correspond to $\sigma = 2.0$ mPa and 32 mPa.

bution in the strength of individual vortex pinning sites at low temperature. Annealing might effectively remove the weakest pinning centers so that the low temperature limiting value of NCRIF is only decreased at small v_0 . At greater speeds these weak regions are irrelevant since there is a plethora of free vortices, hence the convergence in Figs. 2 and 3 at $v_0 > 50 \mu\text{m s}^{-1}$.

In the context of superconductivity or magnetism (or superfluidity), the system is prepared differently if (velocity) field-cooling or zero field-cooling are employed. The hysteresis shown in Figs. 4 and 5 is a consequence of what the authors of Ref. 7 have called vortex glass behavior. If the state of the system is prepared at low v_0 there is only a “small” number of vortices frozen into the solid. When v_0 is gradually increased while $T < T^*$, NCRIF becomes either unstable (see Fig. 4) or metastable (see Fig. 5). In the former case, NCRIF decays until it reaches a metastable state. For $T > T^*$, NCRIF is reduced by the enhanced mobility of vortices.

The low temperature metastability seems to depend on the difference between the initial NCRIF prepared at low speed and the “equilibrium” value obtained upon cooling at the higher speed. For instance, the difference is $\text{NCRIF} = 0.9\%$ for BC-12/10/06 (see Fig. 4) and $\text{NCRIF} = 0.08\%$ for CP-11/21/06 (see Fig. 5), resulting in a much more stable value for the latter. The measured value for BC-12/10/06 immediately drops by about 40% of its magnitude following the increase in v_0 , while there is no

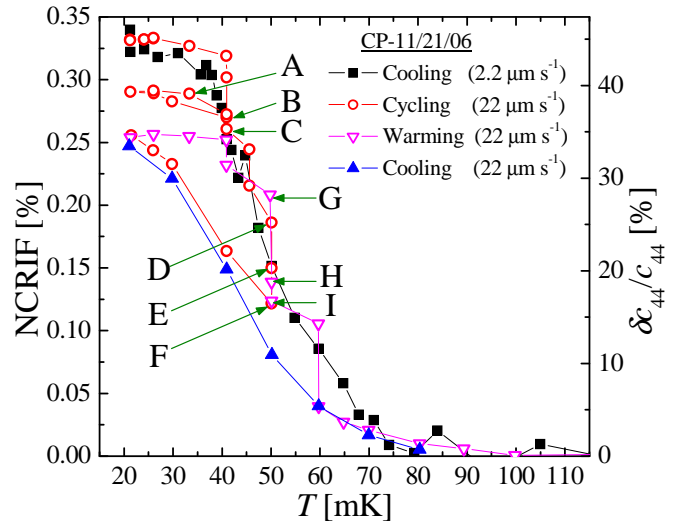


FIG. 5: Metastability of NCRIF and $\delta c_{44}/c_{44}$ for a CP sample. The sample was assumed to be a single crystal with its c-axis oriented horizontally. If we instead assume that the c-axis is oriented vertically (or that the sample is isotropic) the low temperature limiting value of $\delta c_{44}/c_{44}$ would be 60% (30%). Labels A through I denote changes in the decay rate at several different temperatures. The speeds of $v_0 = 2.2 \mu\text{m s}^{-1}$ and $22 \mu\text{m s}^{-1}$ correspond to $\sigma = 3.4$ mPa and 34 mPa.

change for CP-11/21/06. The behavior of CP-11/21/06 is similar to that in Ref. 7, which was compared with the Meissner effect (i.e., a robust NCRIF due to the inability of vortices to enter into the solid). We note that the metastability up to $800 \mu\text{m s}^{-1}$ in Ref. 7 may be related to the small $\text{NCRIF} \approx 0.1\%$ of the sample. In comparison, upon raising v_0 to $880 \mu\text{m s}^{-1}$ we observe, for a 0.3 ppm sample with $\text{NCRIF} > 1\%$ ($\delta f_{He} > 8$ mHz), an abrupt drop in the signal that is followed by a gradual decay. In fact, in this extreme limit of v_0 , the decay rate is essentially insensitive to temperature steps (warming and cooling) between 20 mK and 45 mK. Only upon warming above 60 mK does the decay rate increase further.

In 1 ppb samples, the stability is reduced as the temperature is raised above 30 mK. Fragments of data from scans of CP-11/21/06 are displayed in Fig. 6. The data at any $T < 60$ mK cannot be fit satisfactorily using a simple mathematical formula. For example, the decay at 40 mK in Fig. 6(a) (between points A and B) begins immediately, but slows down abruptly after only 1 h. In Fig. 6(b), NCRIF barely changes in the first hour at the same temperature (data prior to point G). Irregular rates are even more apparent at 50 mK. The decay slows down dramatically when NCRIF crosses (e.g., points E and H) from the region above the low velocity cooling trace to the region below it. This is most obvious in the Fig. 6(b), where the sample was warmed to 50 mK rapidly to result in a larger initial NCRIF. The very different decay rates in these two regions, and the identical temperature dependence in warming and cooling scans, both suggest that there is physical significance to the re-

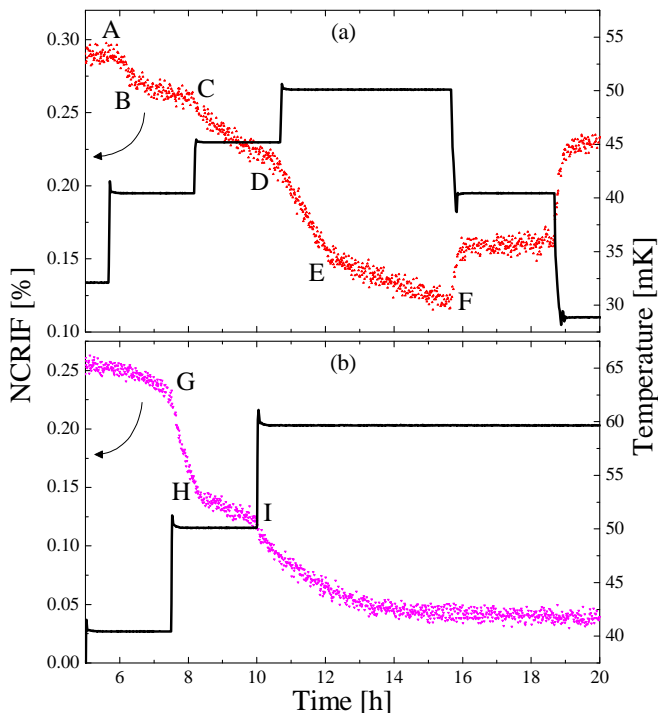


FIG. 6: Segments of raw data used to compile the “cycling” and “warming” curves in Fig. 5. Decay rates above (D to E and G to H) the low velocity trace are greater than those below (E to F and H to I). The ordinate axis is given in terms of NCRIF for easy comparison with Fig. 5.

producible data obtained in the low velocity limit. Similar behavior could not be observed in BC samples because of higher decay rates, i.e., it was impossible to exceed the low velocity trace upon warming (see Fig. 4).

Interestingly, the decay in CP-11/21/06 at 60 mK (data following point I) is different from that at 40 mK and 50 mK in that it can be well fit to an exponential form, which yields a time constant of 2.25 h. The smooth decay across the low velocity trace may indicate that the small tail of NCRIF for $T \geq 60$ mK does not denote the same “boundary” as seen at lower temperatures. This observation is complemented by the enhanced decay rate at 60 mK that we find in 0.3 ppm samples as well as the x_3 -independent specific heat peak that has been observed¹⁹ in the same vicinity, and suggests that there is some inherent transition between the “free” and “pinned” regimes.

Another intriguing result is the nearly equal spacing between each metastable NCRIF among the four samples that we studied in detail (e.g., see Figs. 4 and 5). It is clear that the system prefers to possess specific values of NCRIF in the low temperature limit. For example, counter to the slow decay upon warming a solid sample, as the temperature is lowered we find NCRIF to “jump” up to a steady value (see the data in Fig. 6 following point F). If we naively estimate the frequency shift due to the presence of a single vortex line using the expression²⁸,

TABLE I: Approximate stress amplitudes corresponding to v_C in various cells. Values are estimated by ignoring the effects from the top and bottom surfaces of the cell and equating two different expressions for the torque: $I\alpha = rA\sigma$. Here, α is the angular acceleration and A is the area at the rim of the cell. The stress exerted in an annular geometry differs from that in a cylindrical one by the approximate factor, $(2tf)_{Ann}/(rf)_{Cyl}$.

Cell	f [Hz]	v_C [$\mu\text{m s}^{-1}$]	σ_C [mPa]
Cylinder ^a	1072	< 3.5	< 5.4
Cylinder ^b	1173	15	12
Cylinder ^b	496	15	28
Annulus ^c	912	3-40	1.6-22
Annulus ^d	912	10	5.4
Annulus ^e	874	40	3.3

^aPresent set of measurements.

^bData from Ref. 7.

^cData from Ref. 2.

^dData from Ref. 4.

^eData from Ref. 6.

$I_{Vort} = \pi\rho r^4 \text{NCRIF}/\ln[r/a_0]$, we calculate a shift corresponding to 25% of the observed NCRIF for a vortex core radius²⁹ of $a_0 = 0.1$ nm. This value is of the same order of magnitude to what we observe (e.g., from Fig. 5 we get $0.04/0.33 = 11\%$ for CP-11/21/07).

Although our experimental results can be qualitatively interpreted within the framework of Anderson’s vortex liquid model, very few quantitative comparisons are possible³⁰. One of the present experimental results that is difficult to understand in the vortex picture is depicted in Fig. 3. In two samples the observed frequency shift continues to increase when v_0 is reduced to $1 \mu\text{m s}^{-1}$, such that even the peak to peak amplitude of $2 \mu\text{m s}^{-1}$ is less than that which corresponds to a single quantum of circulation ($\sim 3.5 \mu\text{m s}^{-1}$).

IV. ANOMALOUS ELASTICITY OF SOLID ⁴HE

Due to the similarities discussed in Sec. I between the observed frequency shifts and the results of Ref. 23, we are compelled to interpret the data from Sec. II in terms of the response of the dislocation network to oscillating stress fields imposed on the solid.

Here we report our preliminary estimates of changes in the shear modulus of solid ⁴He. By calculating²⁴ the resonant frequency of the torsion mode for different c_{44} values we extracted the percentage change in the modulus that corresponds to a small frequency shift of the TO. The change is given by $\delta c_{44}/c_{44} = (d\ln f/d\ln c_{44})^{-1}(\delta f_{He}/f)$, where the derivative term comes from the FEM calculation and frequency shift comes directly from our TO measurements. The results of our calculations are shown in Figs. 4 and 5. Since the low temperature change in the resonant frequency is very small (parts per million), it scales linearly with the change in the shear modulus. As

a result the inferred temperature dependence of $\delta c_{44}/c_{44}$ is identical to δf_{He} . It is therefore natural that the qualitative features of the data in Ref. 23 be very similar to that from TO studies.

However, the magnitude of the relative change in c_{44} appears to be different. In order to account for the observed δf_{He} in TO measurements the required $\delta c_{44}/c_{44}$ values among the samples studied are between two and five times larger than those seen in Ref. 23. Moreover, the changes are greater than the theoretical upper limit of 30% that can result from the pinning of dislocation lines³¹. We have carried out similar calculations for some of the TO's in the literature^{2,4,7,32} and found that even larger values of $\delta c_{44}/c_{44}$ are necessary to account for the observed δf_{He} . For instance, typical NCRIF values in Refs. 2,4,32 all translate into an increase in c_{44} by approximately a factor of 10. For the double oscillator from Ref.7 we find c_{44} to increase by factors of 5 and 10 in the anti-symmetric and symmetric modes, respectively. This implies that the effect is very dependent on frequency, contrary to the findings of Day and Beamish. Furthermore, it is difficult to apply the dislocation pinning picture to the experiments in porous Vycor glass¹, in which the dimensions of helium (i.e., the pore size) are smaller than typical dislocation loop lengths in bulk crystals^{18,21,33}. This, and the fact that the crystalline phase³⁴ of the confined ⁴He is body-centered-cubic rather than hexagonal-close-packed, would lead one to expect very different behavior in the response to torsional oscillations, counter to what is observed.

Day and Beamish found the measured shear modulus to be a function of stress amplitude. Below a critical stress σ_C the magnitude of c_{44} saturates at a maximum value, as does δf_{He} in some samples (see Fig. 3). This critical value, $\sigma_C = 300$ mPa, is smaller than the estimated breakaway stress of 4 Pa for a ³He-³He separation of 5 μm (a typical loop length^{18,21,33}) along a dislocation, but closely matches the stress at which δf_{He} tends to zero in Fig. 3. Such strong nonlinearity between the drive and response, also seen in other low frequency acoustic measurements³⁵, occurs at "critical" speeds that are 100 to 1000 times less (e.g., ~ 50 nm s^{-1} in Ref. 23) than in TO studies^{2,4,6,7,8}. It was concluded in Ref. 23 that σ_C is a more fundamental quantity than v_C due to it being independent of the measurement frequency. However, this is inconsistent with Ref. 7 and implies that the two types

of measurements, although clearly related on some level, are distinct.

V. CONCLUSIONS

We have studied a number of solid ⁴He samples grown within a torsional oscillator at constant temperature and pressure, as well as with the blocked capillary method, and found that the resonant frequency of the system possesses a very strong thermal history. The magnitude of the apparent NCRIF measured in the low temperature limit is reproducible when obtained upon cooling the sample from temperatures well above the transition. Modulation of the oscillation speed below the onset temperature reveals the existence of many metastable states.

We find that these properties are qualitatively consistent with two different interpretations: the response of vortices to velocity fields and/or the response of dislocation lines within the solid to oscillating stress fields. The mobility of either of these entities becomes very limited with decreasing temperature, resulting in hysteretic behavior below 60 mK. Extreme pinning takes place below 30 mK (1 ppb) or 45 mK (0.3 ppm), such that their motion is essentially frozen out.

At present there remain discrepancies between the experiments and either of the two interpretations. In the vortex liquid picture, the most notable problem is the very low critical velocity found in this study. In regard to the elastic properties of solid ⁴He, we find that the majority of the frequency shifts observed are appreciably larger than upper limit expected from the pinning of dislocations.

Acknowledgments

We thank P. W. Anderson, J. R. Beamish, W. F. Brinkman, D. A. Huse, J. Jain, H. Kojima, X. Lin, L. Pollet, N. V. Prokof'ev, A. S. C. Rittner, J. Toner, and J. T. West for their input. We are grateful to J. A. Lipa for providing us with isotopically pure ⁴He. Funding was provided by the USA NSF under grants DMR-0207071 and DMR-0706339.

* Electronic address: cctony1@gmail.com

¹ E. Kim and M. H. W. Chan, Nature (London) **427**, 225 (2004).

² E. Kim and M. H. W., Science **305**, 1941 (2004).

³ E. Kim and M. H. W. Chan, J. Low Temp. Phys. **138**, 859 (2005).

⁴ E. Kim and M. H. W. Chan, Phys. Rev. Lett. **97**, 115302 (2006).

⁵ A. S. C. Rittner and J. D. Reppy, Phys. Rev. Lett. **97**,

165301 (2006).

⁶ A. S. C. Rittner and J. D. Reppy, Phys. Rev. Lett. **98**, 175302 (2007).

⁷ Y. Aoki, J. C. Graves, and H. Kojima, Phys. Rev. Lett. **99**, 015301 (2007).

⁸ A. Penzev, Y. Yasuta, and M. Kubota, J. Low Temp. Phys. **148**, 677 (2007).

⁹ M. Kondo, S. Takada, Y. Shibayama, and K. Shirahama, J. Low Temp. Phys. **148**, 695 (2007).

- ¹⁰ A. C. Clark, J. T. West, and M. H. W. Chan, Phys. Rev. Lett. **99**, 135302 (2007).
- ¹¹ E. Kim *et al.*, to be published in Phys. Rev. Lett. (2008); arXiv:0710.3370v1 (2007).
- ¹² A. Penzev, Y. Yasuta, and M. Kubota, arXiv:0711.0212v2 (2007).
- ¹³ P. W. Anderson, Nature Phys. **3**, 160 (2007).
- ¹⁴ We note an error in Refs. 2 and 4, i.e., $t = 0.95$ mm rather than 0.6 mm.
- ¹⁵ ^3He atoms are attracted to vortices in superfluid liquid ^4He due to the lower local density in the vortex core. For this reason it has been suggested that vortices in solid ^4He are nucleated between lattice sites in regions of lower density. For instance, see W. M. Saslow, Phys. Rev. B **71**, 092502 (2005). Repulsion of ^3He atoms from the vortex core is expected if the local density is higher than the average value. This might in fact be applicable to solid ^4He if the super-solid phase is due to a finite concentration of vacancies. For example, see C. Wu, H. Chen, J. Hu, and S. C. Zhang, Phys. Rev. A **69**, 043609 (2004).
- ¹⁶ Z. Nussinov, A. V. Balatsky, M. J. Graf, and S. A. Trugman, Phys. Rev. B **76**, 014530 (2007).
- ¹⁷ A. V. Balatsky, M. J. Graf, Z. Nussinov, and S. A. Trugman, Phys. Rev. B **75**, 094201 (2007). We note that the particulars of the theory are not quite reconciled by the observed frequency dependence of δf . For example, based on the glass parameters obtained from the symmetric mode of oscillation in Ref. 7, the predicted frequency shift of the antisymmetric mode is approximately 10 times smaller than the experimental value.
- ¹⁸ R. Wanner, I. Iwasa, and S. Wales, Solid State Commun. **18**, 853 (1976).
- ¹⁹ Lin, X., A. C. Clark, M. H. W. Chan, Nature (London) **449**, 1025 (2007).
- ²⁰ M. G. Richards, J. Pope, and A. Widom, Phys. Rev. Lett. **29**, 708 (1972); V. N. Grigor'ev *et al.*, J. Low Temp. Phys. **13**, 65 (1973); A. R. Allen, M. G. Richards, and J. Schrat-ter, *ibid.* **47**, 2890 (1982).
- ²¹ I. Iwasa and H. Suzuki, J. Phys. Soc. Jpn. **49**, 1722 (1980).
- ²² M. A. Paalanen, D. J. Bishop, and H. W. Dail, Phys. Rev. Lett. **46**, 664 (1981).
- ²³ J. Day and J. R. Beamish, arXiv:0709.4666v1 (2007).
- ²⁴ An eigenfrequency analysis of the TO was carried out using the Structural Mechanics Module of COMSOL Multiphysics. The entire TO (the base, torsion rod, and torsion bob both with and without ^4He), was drawn in a computer-aided design (CAD) environment, from which a mesh of finite, tetrahedral elements was generated. To perform calculations in a convenient period of time the number of elements was typically limited to less than 30,000. However, meshes with higher densities were also tested in several cases to ensure the accuracy of the resonant frequency. Based only on the dimensions of the TO and the elastic properties of its constituents we found f to be in excellent agreement with the experimental value (i.e., within 1%). Similarly, high accuracy was obtained for the calculated mass loadings of a number of samples (within 2%). Further details of our presently ongoing FEM study will be published elsewhere.
- ²⁵ J. P. Bouchand and G. Biroli, arXiv:0710.3087v1 (2007).
- ²⁶ We discuss the “velocity dependence” in a general sense, in that it is simply proportional to the drive level input to the system (as is amplitude, acceleration, stress, etc.).
- ²⁷ J. E. Vos *et al.*, Physica **37**, 51 (1967).
- ²⁸ G. B. Hess, Phys. Rev. **161**, 189 (1967).
- ²⁹ Due to the logarithmic dependence, the magnitude of the vortex angular momentum is fairly insensitive to a_0 (e.g., taking $a_0 = 100$ nm would reduce the calculated frequency shift by less than a factor of 2).
- ³⁰ A very recent attempt at an in depth analysis has been made in Ref. 12. If we plot our data in the same manner as Fig. 3 in Ref. 12, we observe very different behavior. At present we do not understand this discrepancy. However, it is interesting to note that for such plots we see qualitative differences between CT/CP and BC samples.
- ³¹ We note that Paalanen *et al.*²² previously reported a 40% change in the shear modulus, but this included high temperature data near the melting point where there are likely other stiffening processes to account for (e.g., the presence or absence of thermally activated vacancies).
- ³² Calculations were also done for a TO now being used by Rittner and Reppy. The construction is similar to that used in Ref. 6, but with a slightly simpler design that is easier to accurately model.
- ³³ I. Iwasa, K. Araki, and H. Suzuki, J. Phys. Soc. Jpn. **46**, 1119 (1979).
- ³⁴ D. Wallacher, D., M. Rheinstaedter, T. Hansen, and K. Knorr, J. Low Temp. Phys. **138**, 1013 (2005).
- ³⁵ Yu. Mukharsky, O. Avenel, and E. Varoquaux, J. Low Temp. Phys. **148**, 689 (2007).